

See discussions, stats, and author profiles for this publication at: <https://www.researchgate.net/publication/51722541>

# Structure and Dynamics of Mycobacterium tuberculosis Truncated Hemoglobin N: Insights from NMR Spectroscopy and Molecular Dynamics Simulations

ARTICLE *in* BIOCHEMISTRY · DECEMBER 2011

Impact Factor: 3.02 · DOI: 10.1021/bi201059a · Source: PubMed

---

CITATIONS

12

---

READS

46

## 8 AUTHORS, INCLUDING:



Anne Sebilo

Laval University

3 PUBLICATIONS 12 CITATIONS

[SEE PROFILE](#)



Fanny Meindre

French National Centre for Scientific Research

1 PUBLICATION 12 CITATIONS

[SEE PROFILE](#)



Patrick Lagüe

Laval University

35 PUBLICATIONS 406 CITATIONS

[SEE PROFILE](#)



Michel Guertin

Laval University

59 PUBLICATIONS 3,351 CITATIONS

[SEE PROFILE](#)

# Structure and Dynamics of *Mycobacterium tuberculosis* Truncated Hemoglobin N: Insights from NMR Spectroscopy and Molecular Dynamics Simulations

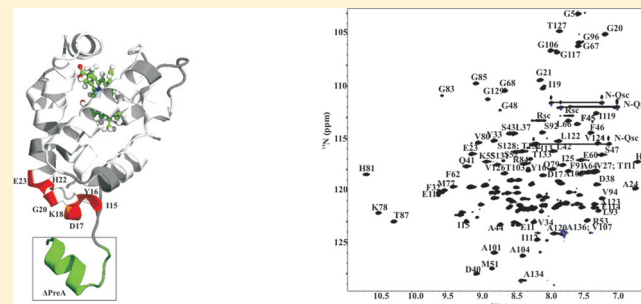
Pierre-Yves Savard,<sup>†</sup> Richard Daigle,<sup>†</sup> Sébastien Morin,<sup>†,§</sup> Anne Sebilo,<sup>†</sup> Fanny Meindre,<sup>‡</sup> Patrick Lagüe,<sup>†</sup> Michel Guertin,<sup>†</sup> and Stéphane M. Gagné\*,<sup>†</sup>

<sup>†</sup>Département de biochimie, de microbiologie et de bio-informatique, Université Laval and PROTEO, Québec, Canada

<sup>‡</sup>Centre de biophysique moléculaire, Orléans, France

## Supporting Information

**ABSTRACT:** The potent nitric oxide dioxygenase (NOD) activity ( $\text{trHbN}-\text{Fe}^{2+}-\text{O}_2 + \bullet\text{NO} \rightarrow \text{trHbN}-\text{Fe}^{3+}-\text{OH}_2 + \text{NO}_3^-$ ) of *Mycobacterium tuberculosis* truncated hemoglobin N (trHbN) protects aerobic respiration from inhibition by  $\bullet\text{NO}$ . The high activity of trHbN has been attributed in part to the presence of numerous short-lived hydrophobic cavities that allow partition and diffusion of the gaseous substrates  $\bullet\text{NO}$  and  $\text{O}_2$  to the active site. We investigated the relation between these cavities and the dynamics of the protein using solution NMR spectroscopy and molecular dynamics (MD). Results from both approaches indicate that the protein is mainly rigid with very limited motions of the backbone N–H bond vectors on the picoseconds–nanoseconds time scale, indicating that substrate diffusion and partition within trHbN may be controlled by side-chains movements. Model-free analysis also revealed the presence of slow motions (microseconds–milliseconds), not observed in MD simulations, for many residues located in helices B and G including the distal heme pocket Tyr33(B10). All currently known crystal structures and molecular dynamics data of truncated hemoglobins with the so-called pre-A N-terminal extension suggest a stable  $\alpha$ -helical conformation that extends in solution. Moreover, a recent study attributed a crucial role to the pre-A helix for NOD activity. However, solution NMR data clearly show that in near-physiological conditions these residues do not adopt an  $\alpha$ -helical conformation and are significantly disordered and that the helical conformation seen in crystal structures is likely induced by crystal contacts. Although this lack of order for the pre-A does not disagree with an important functional role for these residues, our data show that one should not assume an helical conformation for these residues in any functional interpretation. Moreover, future molecular dynamics simulations should not use an initial  $\alpha$ -helical conformation for these residues in order to avoid a bias based on an erroneous initial structure for the N-termini residues. This work constitutes the first study of a truncated hemoglobin dynamics performed by solution heteronuclear relaxation NMR spectroscopy.



Tuberculosis infects one-third of the world's population. Most infected individuals fail to progress to complete disease because the TB bacilli are maintained in a latency state by the immune system. During latent infection mycobacteria are exposed to low  $\text{O}_2$  concentrations and to nitric oxide ( $\bullet\text{NO}$ ) produced by the immune system of the host. Since  $\bullet\text{NO}$  can inhibit or inactivate key enzymes such as the terminal respiratory oxidases and the iron/sulfur protein aconitase and can generate secondary reactive nitrogen species displaying varied reactivity and toxicity,<sup>1–7</sup>  $\bullet\text{NO}$ -metabolizing reactions are thus required for *Mycobacterium tuberculosis* (*Mtb*) to fight  $\bullet\text{NO}$  poisoning. The truncated hemoglobin N (trHbN) from the pathogenic bacterium *Mtb* has a potent ability to detoxify  $\bullet\text{NO}$  to nitrate (nitric oxide dioxygenase reaction (NOD)) and to protect aerobic respiration from the inhibition by  $\bullet\text{NO}$  in stationary phase cells of *M. bovis* BCG.<sup>8</sup> The high rate of  $\bullet\text{NO}$  oxidation ( $k_{\text{NOD}} \approx 745 \mu\text{M}^{-1} \text{s}^{-1}$  at 23 °C) catalyzed by

oxygenated trHbN and the large affinity ( $K_d = 8 \text{ nM}$ ) for  $\text{O}_2$  suggest that the NOD reaction may be one of the vital defense systems in *Mtb* for coping with the toxic effects of  $\bullet\text{NO}$  under the low  $\text{O}_2$  concentration (1–4  $\mu\text{M}$ ) prevailing in infected lesions.<sup>9</sup> An understanding of the structure and dynamics characteristics leading to this high reactivity is essential; hence the need to study the molecular mechanisms controlling ligand/substrate access to the distal heme pocket (DHP).

A striking feature of trHbN is the presence of multiple narrow hydrophobic tunnels connecting the active site to distinct protein surface sites. Figure 1 shows the tunnels that have been identified using MD simulations<sup>10</sup> and X-ray crystallography:<sup>11</sup> short tunnel (ST), long tunnel (LT), EH

Received: July 9, 2011

Revised: October 7, 2011

Published: October 17, 2011

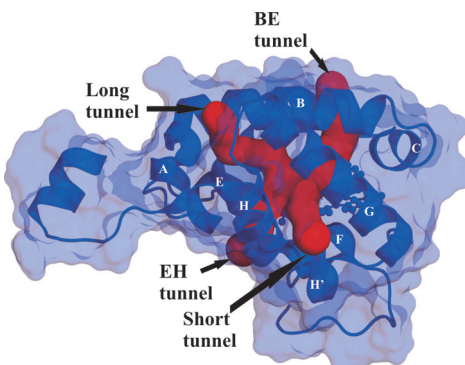


**Figure 1.** Structure of trHbN displaying the four tunnels: long tunnel (LT), short tunnel (ST), EH tunnel, and BE tunnel.

tunnel (EHT), and BE tunnel (BET). These tunnels are not open channels but are formed of short-lived hydrophobic neighboring cavities of various shapes and volumes<sup>10</sup> that partition substrates from solvent. These cavities are temporally interconnected due to side-chain flexibility. The high rigidity of trHbN backbone as observed in MD simulations<sup>10</sup> enables these numerous cavities. Interestingly, except for one, all these cavities correspond to the Xe binding pockets identified by X-ray crystallography.<sup>11</sup> Dynamic hydrophobic tunnels of narrow diameter, as observed in trHbN, may also prevent the formation of hydrogen-bonded water clusters that can hinder passage of other molecules through the tunnel. Water molecules and other polar substrates in hydrophobic tunnels typically have very rapid subnanosecond transit times that ensure that water will not hinder passage of less polar substrates. In contrast to the Xe cavities in myoglobin, the hydrophobic tunnels in trHbN constitute the trajectory linking the DHP to the solvent.<sup>10,12–15</sup>

As we reported earlier, the local entrance of the tunnels also contributes to the overall reactivity both through substrate selectivity and through the dynamics controlling the transit between the external solvent and the internal tunnel.<sup>12</sup> The hydrophobicity and polarity of the cluster of residue side-chains localized at the tunnel entrance can create domains that favor local enhancements in the concentration of potential substrates.<sup>12</sup> Reactants such as •NO are soluble in aqueous environments but have higher solubility in hydrophobic environments. Thus, hydrophobic patches in the region of the tunnel entrance on an otherwise hydrophilic/polar surface may serve to create an enhanced buildup of •NO at the proposed site of entry. Our recent results<sup>12</sup> show •NO molecules interacting with oxygenated trHbN preferentially at the entrance of the tunnels. In trHbN the hydrophobic nature of the entrances forces water molecules partitioning away from the protein surface and thus favors •NO capture.

A functional consequence of the tunnels is that •NO reaches the bound O<sub>2</sub> without the need for important structural changes, allowing trHbN to catalyze NOD reaction at a rate approaching that of diffusion-controlled reactions. Interestingly, myoglobin requires the distal His64(E7) to swing out of the DHP, resulting in a much slower NOD activity ( $k_{\text{NOD}} \approx 45 \mu\text{M}^{-1} \text{s}^{-1}$  at 23 °C).

Another unusual feature of trHbN is the presence of the so-called pre-A helix, located at the N-terminus. This “floating” tail was recently assigned a functional role by influencing the diffusion of ligands to the active site.<sup>16</sup> The authors proposed that the deletion of the pre-A helix alters protein dynamics,

especially the conformational state of the Phe62(E15) residue restricting the passage of NO to the DHP, thus affecting the ability of trHbN for •NO detoxification.<sup>16</sup> However, since the protruding and rigid conformation of the pre-A helix observed in the crystal lattice could be questionable, it may be ill-advised to interpret the functional role of the pre-A helix based on the unusual conformation observed in the crystal structure.

To this day, no experimental data are available on the structure and dynamics of trHbN in solution. The present work describes the first heteronuclear relaxation study of a truncated hemoglobin by solution NMR spectroscopy. The structure and dynamics of trHbN in the cyanomet form were studied using NMR chemical shifts, relaxation data acquired at three magnetic fields, and NMR amide exchange experiments. The cyanomet form was studied since the majority of currently available structures for trHbN, including the structure with Xe atoms highlighting the tunnel network, were obtained in complexes with cyanide in the ferric state, and that cyanide represents a valuable diatomic ligand model system. In order to evaluate the structural integrity of the pre-A helix in solution, we have studied both the wild-type protein and the Δpre-A mutant in the cyanomet form. To complement the NMR data, the characterization was carried out in combination with MD simulations.

## MATERIALS AND METHODS

**NMR.** *Protein Expression, Labeling, and Purification.* The genes coding for the mature wild-type trHbN protein (136 residues) as well as for the Δpre-A mutant (lacking residues 1–12) were cloned in *E. coli* BL21(DE3) cells. Proteins were prepared by reconstitution of the apoprotein with heme in a manner similar to the one described by Scott and Lecomte.<sup>17</sup> Details of protein preparation methods can be found in the Supporting Information.

**Samples Preparation and NMR Spectra Recording.** <sup>15</sup>N- or <sup>15</sup>N/<sup>13</sup>C-uniformly labeled protein samples were prepared at a concentration of 0.8 mM in a 20 mM KPO<sub>4</sub> pH 7.5 buffer containing 50 μM EDTA, 3 mM KCN, 10% D<sub>2</sub>O, 1X Complete protease inhibitors (Roche), and 0.1 mM DSS. All experiments were performed at 26.4 °C (calibrated using MeOH) on Varian INOVA 600 (Université Laval, Québec, Canada), 500, and 800 (Québec/Eastern Canada High Field NMR Facility, McGill University, Montréal, Canada), all equipped with z-axis, pulsed-field gradient, triple-resonance cold probe.

**NMR Resonance Assignment.** For backbone and side-chains resonances assignment, the following spectra were collected using pulse sequences from Biopack (Varian Inc., Palo Alto, CA): 2D <sup>15</sup>N-HSQC, 2D <sup>13</sup>C-HSQC (both aliphatic and aromatic), 3D HNCO, 3D CBCA(CO)NH, 3D HNCACB, 3D C(CO)NH, 3D HC(CO)NH, 3D HCCH-TOCSY, 3D <sup>13</sup>C-NOESY-HSQC, and 3D HNHB. All these experiments were performed on a Varian INOVA 600 spectrometer (Université Laval, Québec, Canada). All spectra were processed using NMRPipe/NMRDraw<sup>18</sup> and analyzed within NMRView.<sup>19</sup>

**<sup>15</sup>N Spin Relaxation Experiments.** <sup>15</sup>N-R<sub>1</sub>, <sup>15</sup>N-R<sub>2</sub>, and {<sup>1</sup>H}-{<sup>15</sup>N} NOE NMR relaxation experiments were recorded at proton frequencies of 500, 600, and 800 MHz. Pulse sequences from the Kay group were used.<sup>20,21</sup> More details are available in the Supporting Information.

**Model-Free Analysis.** The model-free analysis<sup>22,23</sup> was performed using an axially symmetric diffusion tensor within the program MODELFREE 4.20 (A.G. Palmer III, Columbia

University, New York, NY). Details are available in the Supporting Information.

**Amide Exchange Experiments.** Amide exchange experiments were performed as described in Morin and Gagné.<sup>24</sup> Data were recorded at 600 MHz at both pH 7.5 and 8.5. At pH 7.5, a total of 45 <sup>15</sup>N-TROSY-HSQC spectra (BIOPACK, Varian, Palo Alto, CA) were recorded. Details can be found in the Supporting Information.

**Molecular Dynamics Simulations.** Force field optimization of the cyanide-bound heme atomic charges and Fe–C–N angle parameter CHARMM22<sup>25</sup> force field lacks parameters for the cyanide-bound heme. To simulate CN-bound trHbN in this study, the atomic charges of heme prosthetic group as well as the cyanide and the Fe–C–N angle parameter were optimized following the standard parametrization protocol for the CHARMM22 force field.<sup>25</sup> The same procedure was previously applied for O<sub>2</sub>-bound heme force-field parameters,<sup>10</sup> and details are given in the Supporting Information.

**Systems and Simulation Setup.** Initial coordinates were taken from wild-type cyanomet trHbN crystallographic structure (PDB 1 RTE).<sup>14</sup> Crystallographic water and sulfate ions were ignored. Hydrogen atoms were added using CHARMM's HBUILD facility.<sup>26</sup> All ionizable residues were considered in their standard protonation state at pH 7.0 with neutral histidine protons placed at the ND1 position. The crystal unit cell contained two trHbN molecules (A and B chains). Both chains were used individually to start two independent 85 ns MD simulations in order to increase sampling (trajectories identified hereafter as A-trHbN and B-trHbN). The first 5 ns were considered as equilibration time. The complete protocol is available in the Supporting Information.

**Trajectory Analysis.** The protein N–H bond S<sup>2</sup> parameters were calculated using the M2 method described in Fisette et al.<sup>27</sup> Briefly, method M1 was used to verify convergence of the backbone amide autocorrelation function ( $C_1(t)$ ) (approximating the ensemble using the last 80 ns of simulations for  $t < 40$  ns). When a function did not converge, S<sup>2</sup> was estimated as the average of the last 500 ps. In M2 method, all structure snapshots from the two trajectories were combined and randomized. The correlation function decays to its plateau value immediately after  $C_1(0)$ . The S<sup>2</sup> estimate therefore takes into account 160 ns of simulation time.

Backbone amide group accessible surface area (ASA) was calculated using a probe radius of 1.4 Å at every 10 ps. Backbone amide hydrogen bond occupancy was analyzed with various N–H acceptor distance cutoffs (2.0, 2.2, and 2.4 Å) and a minimum N–H acceptor angle of 120°.

## RESULTS

**NMR. Protein Expression, Labeling, and Purification.** Using the protocol described in the Supporting Information, ~20 mg of highly pure reconstituted trHbN (r-trHbN) per liter of M9 medium was obtained for the wild-type protein and ~80 mg per liter for the reconstituted Δpre-A mutant (Δpre-A r-trHbN). According to LC-MS analysis, incorporation of <sup>13</sup>C and <sup>15</sup>N in our samples was ≥96%. The samples were stable for several weeks at room temperature. Kinetics parameters for O<sub>2</sub> and CO binding and dissociation of r-trHbN were determined (data not shown) and found identical to those already published. Resonance Raman spectra for the O<sub>2</sub> and CO r-trHbN complexes also indicate that the DHP is quite identical to that of trHbN. Dynamic light scattering measurements were

made at several concentrations to ensure that there was no aggregation/oligomerization in the NMR sample. The protein was found as a monomer in solution at the concentration used for NMR. We also noticed that Met1 was cleaved for the wild-type protein but was still present for the Δpre-A mutant, as confirmed by mass spectrometry.

**<sup>1</sup>H, <sup>15</sup>N, and <sup>13</sup>C Resonance Assignments for trHbN Cyanomet.** As shown in Figure 2, the 2D <sup>15</sup>N-HSQC

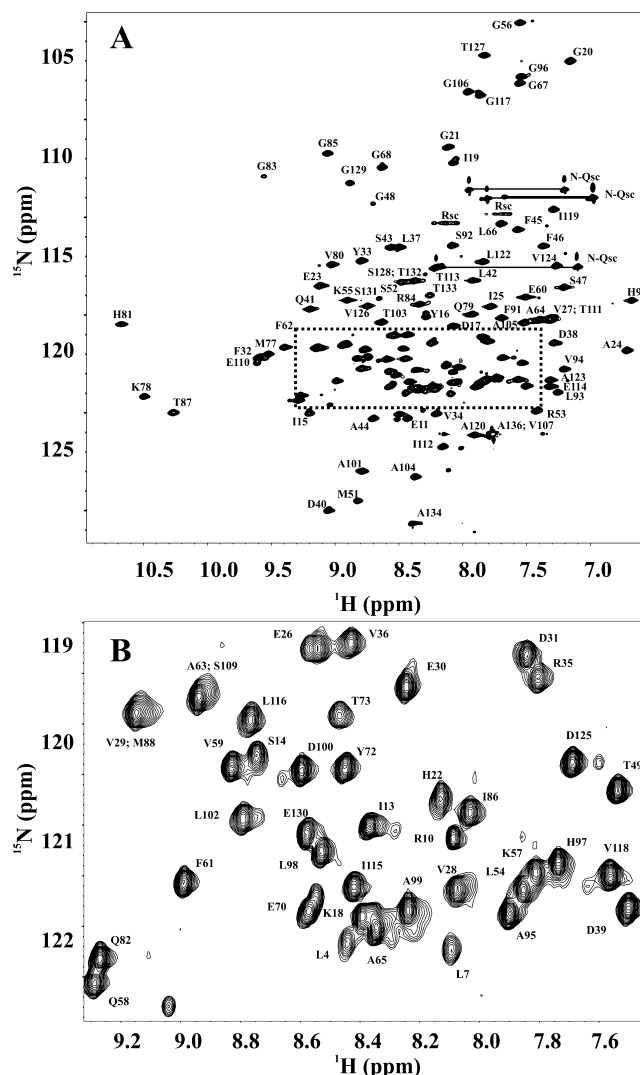


**Figure 2.** (A) Assigned <sup>1</sup>H-<sup>15</sup>N HSQC spectrum of trHbN cyanomet, 0.7 mM, pH 7.5, acquired at 600 MHz, 26.4 °C. (B) Zoom of the most crowded region of the spectrum.

spectrum of r-trHbN cyanomet is of high quality, with a good dispersion of the N–H resonances. Backbone resonance assignment was completed for cyanomet r-trHbN at 97%, 99%, 96%, and 96% respectively for backbone amides, C<sub>α</sub>, C<sub>β</sub>, and carbonyls. Missing amide assignments are for Leu3, Arg6, Lys9, and Gly74 as well as for the 7 proline residues (Pro12, Pro69, Pro71, Pro76, Pro108, Pro121(H13), and Pro135). Most of the missing amides are located in the pre-A region of the protein (residues 2–9) as they were too weak to be visible in the spectra. Assignment for the amide group of Gly74 was not possible because of overlapping with other glycine residues. Missing assignments for C<sub>α</sub> are for Gly2 and Ser5. For C<sub>β</sub>, missing assignments are Ser52(E5), Val107(GH5), and

Ser109(H1). Finally, missing assignments for carbonyls are Gly2, Leu4, Ser5, Arg8, Arg53(E6), and Thr73. For side-chains, 75% of the resonances assignment was completed. Chemical shifts have been deposited in the Biological Magnetic Resonance Data Bank (BMRB) under accession number 17226.

**<sup>15</sup>N Spin Relaxation Data.** <sup>15</sup>N spin relaxation data were recorded at three magnetic fields (500, 600, and 800 MHz proton Larmor frequencies) in order to better characterize the dynamics of r-trHbN in solution. Mean values for <sup>15</sup>N- $R_1$ , <sup>15</sup>N- $R_2$ , and {<sup>1</sup>H}-<sup>15</sup>N NOE are presented in Table 1, and all

**Table 1. Average  $R_1$  and  $R_2$  Relaxation Rates ( $s^{-1}$ ) and {<sup>1</sup>H}-<sup>15</sup>N NOEs at 500, 600, and 800 MHz<sup>a</sup>**

	500 MHz	600 MHz	800 MHz
<sup>15</sup> N- $R_1$	2.05 ± 0.16	1.22 ± 0.11	0.93 ± 0.12
<sup>15</sup> N- $R_2$	12.43 ± 2.38	13.36 ± 2.76	not used <sup>b</sup>
{ <sup>1</sup> H}- <sup>15</sup> N NOE	0.66 ± 0.37	0.70 ± 0.31	0.77 ± 0.21

<sup>a</sup>Mean value with associated SD for all the data available at three fields (101 residues). <sup>b</sup> $R_2$  acquired at 800 MHz were not used in our analysis as they were shown by consistency tests<sup>42</sup> to be inconsistent with  $R_2$  acquired at 500 and 600 MHz. This was done in order to prevent artifactual conclusions to be drawn from the data. More details are available in the Supporting Information.

experimental values are plotted in Figure 3A–D. Values obtained are homogeneous and show the same pattern for all the magnetic fields, with smaller  $R_2$  for residues in N- and C-termini and in loops, as expected for these more mobile regions. Raw relaxation data for each residue at the three fields are available in Table S2 of the Supporting Information. <sup>15</sup>N spin relaxation data for r-trHbN have been deposited in the BMRB under accession number 17226.

**Model-Free Analysis.** It was possible to get high-quality data for 101 out of the 127 non-proline observable residues at the lowest magnetic field of 500 MHz, overlapping or too broad resonances being responsible for nonanalyzed amides. Only these 101 residues which have data at the three magnetic fields were used to perform the model-free analysis.

Examination of the inertia tensor of r-trHbN indicates an asymmetric protein, with relative moments of 1.00:0.96:0.45. Many diffusion tensors were tested, using either the program relax<sup>28,29</sup> (local  $\tau_m$ , sphere, prolate spheroid, oblate spheroid, and ellipsoid) or Quadric (A. G. Palmer III, Columbia University) (isotropic, axial, and anisotropic). The best model appeared to be prolate spheroid with relax and axial with Quadric, which are mostly the same. Consequently, an axially symmetric (spheroid) tensor was used for the model-free analysis. Global optimization of the tensor showed that trHbN tumbles anisotropically in solution with a  $D_{||}/D_{\perp}$  value of 1.45 and a global tumbling time of 10.0 ns, similar to the results obtained for other globins of the same size and shape.<sup>30</sup>

For local motions, the data were fitted to the five following model-free models: (m1) [ $S^2$ ], (m2) [ $S^2, \tau_e$ ], (m3) [ $S^2, R_{ex}$ ], (m4) [ $S^2, \tau_e, R_{ex}$ ], (m5) [ $S_f^2, S_s^2, \tau_e$ ], where  $S^2$  (=  $S_f^2 S_s^2$ ) is the square of the generalized order parameter characterizing the amplitude of internal motions,  $S_f^2$  and  $S_s^2$  are the squares of the order parameters for the internal motions on the fast (picoseconds) and slow (nanoseconds) time scales, respectively,  $\tau_e$  is the effective correlation time for internal motions, and  $R_{ex}$  is an additional parameter added to contributions to observed  $R_2$  from conformational exchange and pseudo-first-order processes occurring on the microsecond-to-millisecond

time scale.<sup>31</sup> Following the final model-free model selection step, 46 residues were fitted with model m1, 23 with model m2, 9 with model m3, 6 with model m4, and 17 residues with model m5. Models m1 and m2 are the simplest models and were used to fit most of the residues. These models are representative of residues exhibiting fast pico- to nanoseconds motions for their N–H vectors. Results from the model-free analysis are presented in Table S3.

**NMR Order Parameters,  $S^2$ .** The  $S^2$  generalized order parameter characterizes the amplitude of internal picoseconds–nanoseconds time scale motions of N–H bond vectors.  $S^2$  values vary from 0 for a completely disordered vector to 1 for totally restricted vector.<sup>32</sup>  $S^2$  values obtained for r-trHbN are plotted in Figure 3E and mapped onto the protein structure in Figure 4A. Considering all residues, an average order parameter ( $S^2$ ) of 0.84 was obtained for r-trHbN. In particular, we see that helices B and E are the most rigid of the protein with an average  $S^2$  value of 0.91, which is higher than the average value of 0.88 reported for  $\alpha$ -helices by Goodman et al.<sup>33</sup> Helices F and G appeared to be the most flexible, with average  $S^2$  of 0.84 and 0.86, respectively. Order parameters for other helices are typical.

As expected, a lower degree of motion restriction was observed for loops as well as for both N- and C-termini, for which a very high degree of mobility is observed with average  $S^2$  values of 0.42 and 0.21, respectively.  $S^2$  order parameters for r-trHbN have been deposited in the BMRB under accession number 17226.

**Slow Motions.** The  $R_{ex}$  term in model-free models m3 and m4 accounts for slow microseconds to milliseconds motions. Fifteen residues of r-trHbN were fitted with one of these models, indicating the presence of chemical exchange occurring in the slow microseconds to milliseconds time scale in the vicinity of these residues (Glu30(B7), Tyr33(B10), Gly83, Thr87(G1), His90(G4), Phe91(G5), Val94(G8), Ala95(G9), Leu98(G12), Ala99(G13), Ala101(G15), Leu102(G16), Ala105(G19), Ile112(H4)) (see Figures 3F and 4B). Most of these slow motions are observed for N–H bond vectors of residues located in helices B and G and pointing toward the active site of the protein, some of them located directly in or at the entrance of a tunnel. Active site residues requiring an  $R_{ex}$  term include Tyr33(B10) and Val94(G8) while residues defining tunnel entrances include Phe91(G5) and Ala95(G9) for the ST tunnel and Glu30(B7) and Ty33(B10) for the BET tunnel.

**Two-Time Scale Motions.** Seventeen residues were better characterized by using model m5 (Leu7, Glu11, Ile13, Ala24(B1), Ala44, Glu70, Ala75, Gln79, Val80(F7), Arg84, Gly106, Asp125, Gly129, Glu130, Thr133, Ala134, Val136), indicating the presence of motions occurring at two different time scales ( $S_f^2 = ps$ ,  $S_s^2 = ns$ ) for these N–H vectors. All these residues are located in flexible regions of the protein such as N- and C-termini, loops, or at the beginning of helices.

**NMR Amide Exchange Experiments.** Amide protons can exchange using one of two regimes: EX1 or EX2.<sup>4f</sup> In the EX1 regime, exchange rates are pH independent and give kinetics information on the exchange process; i.e., the exchange rate ( $k_{ex}$ ) is equal to the opening rate for the local structure protecting the N–H group from solvent access ( $k_{op}$ ). In the EX2 regime,  $k_{ex}$  = thermodynamics information can be extracted from pH-dependent exchange rates. The extracted information provides the following parameters, which correspond to different ways to present the same information:  $\Delta G_{HX}$

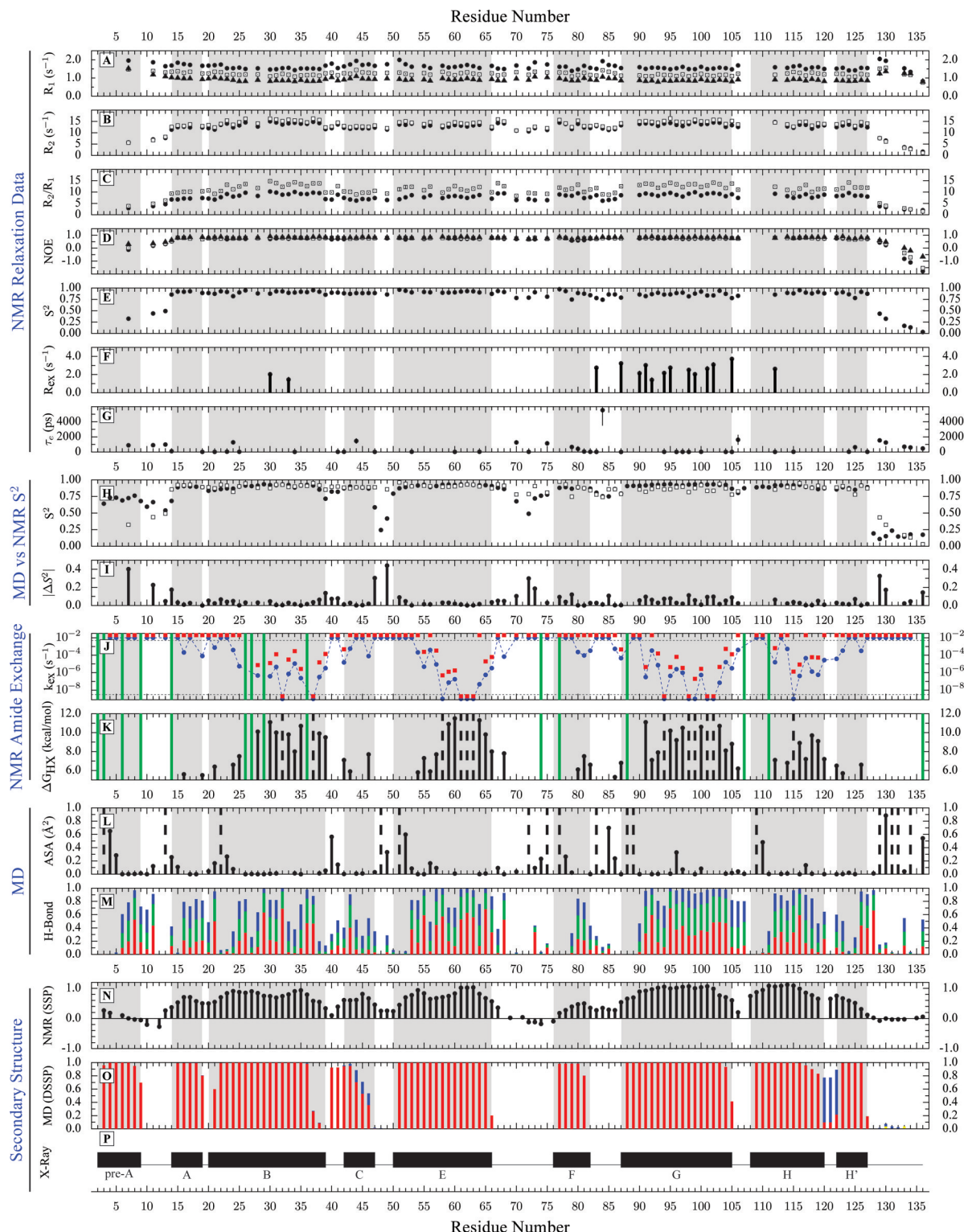


**Figure 3.** (A–D) NMR raw relaxation data ( $R_1$ ,  $R_2$ ,  $R_2/R_1$ , NOE) at 500 (black solid circles), 600 (gray solid squares), and 800 MHz (black solid triangles). (E–G) Model-free parameters ( $S^2$ ,  $R_{\text{ex}}$ , and  $\tau_e$ ) for trHbN cyanomet. (H–I) Comparison of  $S^2$  parameters obtained either from NMR (white solid squares) or MD simulations (black solid circles). (J, K) NMR amide exchange data: amide exchanges rates ( $k_{\text{ex}}$ ) at pH 7.5 (blue circles) and 8.5 (red squares), and free energy for the opening of the protecting structure ( $\Delta G_{\text{HX}}$ ) at pH 7.5. (L, M) Molecular dynamics data: average backbone ASA and backbone amide hydrogen bond occupancy calculated with various cutoffs for the N–H acceptor bond distance. Cutoffs used are 2.0 Å (red), 2.2 Å (green), and 2.4 Å (blue). (N–P) Secondary structure of trHbN calculated by NMR (HN, N, CA, CB chemical shifts used in the program SSP), MD, or taken from the X-ray structure PDB 1S61B.<sup>11</sup>

(the free energy for the opening of the local structure protecting the N–H group),  $K_{\text{op}}$  (the equilibrium constant), and PF (the protection factor for the exchange,  $K_{\text{op}} = 1/\text{PF}$ ).

Generally, under nondenaturing conditions (i.e., high stability), amide protons exchange from the EX2 regime. A simple approach for determination of the exchange regime consists in

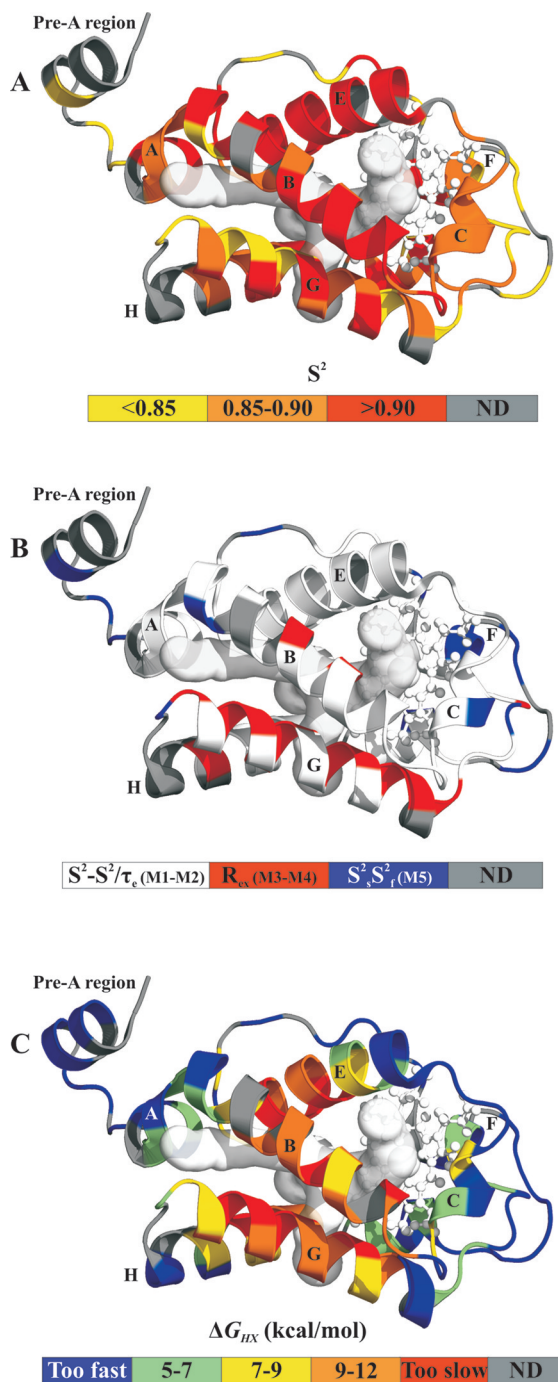


**Figure 4.** Mapping of NMR experimental results on the structure of trHbN. (A) Mapping of the  $S^2$  values. (B) Mapping of residues exhibiting slow motions ( $R_{\text{ex}}$  term, model-free models m3 and m4) (red), two time scale motions ( $S_t^2$  and  $S_s^2$ , m5) (blue) or fitted with simple models ( $S^2$  or  $S^2 - \tau_e$ ) (white). Gray residues represent residues for which no data were available. (C) Mapping of the free energy for the opening of the protecting structure ( $\Delta G_{\text{HX}}$ ). Residues for which data are unavailable (N-terminus, Pro, unassigned, ambiguous and overlapped) are colored gray, while residues with exchange rates too fast ( $k_{\text{ex}} > 10^{-3} \text{ s}^{-1}$ ) and too slow ( $k_{\text{ex}} < 10^{-9} \text{ s}^{-1}$ ) to be characterized are colored either blue or red.

measuring exchange rates at two pH. If rates from the highest pH are faster, then the exchange proceeds using the EX2 regime at the lowest pH. As can be seen from Figure 3, J, amide exchange at pH 7.5 proceeds from the EX2 regime. Indeed, the

rates at pH 8.5 are in average  $30 \pm 10$  times faster than rates at pH 7.5 (while theory would suggest a difference of  $10\times$  between rates from both pH). The faster than expected rate at pH 8.5 could be explained by a slightly less stable structure at pH 8.5, which would result in faster exchange rates for some residues. From these data,  $\Delta G_{\text{HX}}$ ,  $K_{\text{op}}$ , and PF can be extracted to characterize the exchange process at pH 7.5. Figure 3K shows a plot of  $\Delta G_{\text{HX}}$  values according to the residue number, and these values are mapped on the protein structure on Figure 4C. Quantitative data are available for only 52 residues, while semiquantitative data are available for 60 residues (12 too slow, 48 too fast for being quantified). The pre-A region appears as the less stable portion in trHbN. Indeed, from the 5 residues that could be characterized in the pre-A region, neither had a measurable exchange rate; i.e., all exchanged too fast to be characterized. This means that N-H groups in this region are poorly protected from exchange, with  $\Delta G_{\text{HX}}$  lower than 5 kcal/mol. This is in agreement with missing resonances and very low  $S^2$  values observed for this part of the protein. Other short helices such as the A, C, F, and H' helices have low  $\Delta G_{\text{HX}}$ . On the contrary, helices B, E, G, and H have  $\Delta G_{\text{HX}}$  of higher value, even including residues for which exchange rates could not be measured accurately due to the limited time allowed for exchange ( $\sim 42$  days). Exchanging on an intermediate time scale, the H helix has  $\Delta G_{\text{HX}}$  between 7 and 10 kcal/mol. Amide exchange data have been deposited in the BMRB under accession number 17226.

**NMR Investigation of the Δpre-A Mutant.** A recent study concluded that the pre-A region may play an important function by altering the dynamics of the protein core and thus ligand diffusion.<sup>16</sup> In the latter work, the excision of pre-A region triggered changes in LT dynamics, especially for Phe62(E15) side-chain, leading to the blockade of the LT and NO access to the heme-bound oxygen. To validate these conclusions, we generated a mutant protein corresponding to the pre-A mutant described in ref 16 (lacking residues 1–12) and investigated its structure and dynamics by NMR spectroscopy. Δpre-A r-trHbN showed identical kinetic binding properties to r-trHbN. Comparison of <sup>15</sup>N-HSQC from the wild-type and the Δpre-A mutant indicated that changes in the electronic environment are limited to residues neighboring the mutation site. Analysis of the C $\beta$  side-chain chemical shifts revealed that only two residues had significant chemical shift change upon pre-A deletion: Asp17 (0.23 ppm) and His22 (0.34 ppm). Asp17 C $\beta$  is near the deletion and 6.6 Å from the terminal NH<sub>3</sub><sup>+</sup> in the deletion mutant. On the other hand, His22 is far from pre-A residues in the crystal structure (nearest group is the charged extremity of Arg6 at 9.2 Å). We therefore found little evidence that the pre-A region was interacting strongly with other parts of the protein. Figure 5 illustrates the chemical shifts differences ( $\Delta\delta$ ) between the <sup>1</sup>H<sup>15</sup>N resonances from r-trHbN and Δpre-A r-trHbN.

**Solution Structure of the Pre-A "Helix".** As shown in Figure 3E, all N-termini residues up to residue 13 have low order parameters, with steadily decreasing order parameters going toward the N-termini as typically seen in unstructured extremities of several proteins. The region includes the so-called pre-A "helix" that was observed in all trHbN crystal structures. In order to evaluate the helical character of the pre-A region in solution, we have used the program SSP, which uses NMR chemical shifts to calculate a single residue-specific secondary structure propensity score.<sup>34</sup> As shown in Figure 3N, the score obtained for pre-A residues in trHbN is around 0,

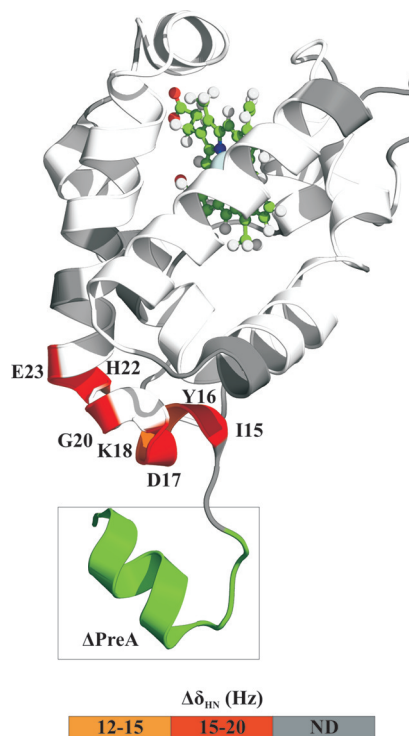


**Figure 5.** Mapping of the chemical shift differences between the wild-type and the  $\Delta$ Pre-A mutant. The cleaved region is shown in green. Chemical shift changes are given in Hz from 600 MHz data and calculated as  $\Delta\delta_{\text{HN}} = (\Delta\delta_{\text{H}}^2 + \Delta\delta_{\text{N}}^2)^{1/2}$ .

implying an absence of  $\alpha$ -helical secondary structure predisposition in solution, consistent with our NMR spin relaxation and amide exchange data.

**Molecular Dynamics Simulation and Comparison with NMR Results.** Stable trajectories were obtained in both molecular dynamics simulations performed. Average backbone root-mean-square deviation (rmsd) for residues in  $\alpha$ -helices stabilized at  $\sim 0.7$  Å.

**MD Order Parameters of N–H Bond Vectors.** Both MD trajectories were used to calculate the generalized order parameter  $S^2$  for backbone N–H bonds (sampling from a total of 160 ns). Comparisons between MD and NMR data are shown in Figure 3H–I.  $S^2$  values, N–H bond internal autocorrelation function, and local motions are available in Table S4 and Figure S1. Individual MD simulations produced very similar  $S^2$  data sets. Significant  $S^2$  differences between these two simulations are observed for the pre-A region and for some residues located in C–E and E–F loops. For some residues located in loops, the autocorrelation function  $C_1(t)$  did not converge during simulations (residues Asp39, Glu70, Gly74).  $S^2$  estimates for these residues would have required more and/or longer MD simulations to converge.

$S^2$  obtained from MD simulations are in very good agreement with those obtained from NMR, as shown in Figure 3H–I. The average MD  $S^2$  obtained for the four  $\alpha$ -helices forming the 2-on-2 fold and enclosing the tunnels (B, E, G, and H helices;  $S^2$  of 0.89) is the same as from NMR and reflects very restricted motions in the picoseconds–nanoseconds time scale. The rmsd between MD and NMR is 0.10 using all residues, 0.16 for loop residues, and 0.06 for residues in  $\alpha$ -helices. Similar agreements were obtained in a recent study on the of *E. coli*  $\beta$ -lactamase TEM-1.<sup>27</sup> The main discrepancy

concerns the pre-A region where MD-derived  $S^2$  are much higher than those obtained from NMR for the two residues that were characterized. Other discrepancies concern some residues located within C–E and E–F loops. These latter discrepancies are explained by the nonconvergence of the autocorrelation function for several residues.

Further agreement of results from NMR and MD concerns residues exhibiting two time scale motions. Of the 17 residues fitted with model m5 in the model-free analysis (two-time scale motions on the picoseconds–nanoseconds time scale), nine were observed to have similar motions in MD simulations. This is shown in MD simulations by N–H vectors exploring more than a single conformation (see residues Glu11, Ile13, Glu70, Arg84, Gly106, Gly129, Glu130, Thr133, and Ala134 in Figure S1).

**Hydrogen Bond Occupancies Compared to Amide Exchange Rates.** Backbone N–H hydrogen bond occupancy was calculated for the different simulations and is shown in Figure 3M. As expected, occupancy is higher in regions with well-formed secondary structure. Particularly, higher occupancies are found in helices E and G correlated with slower amide exchange rates. As for  $S^2$  parameters, however, discrepancies are found for the pre-A region. Indeed, the pre-A region remained structured as an  $\alpha$ -helix along MD simulations, and thus high H-bond occupancies (Figure 3M) and low solvent exposure (Figure 3L) were calculated. This is in striking contrast with the very fast experimental amide exchange rates.

## ■ DISCUSSION

To this day, the structure and dynamics of trHbN have been studied by several techniques such as X-ray crystallography, resonance Raman spectroscopy, or MD simulations. The present work presents the first dynamics study of trHbN using heteronuclear relaxation NMR spectroscopy.

NMR data indicate that the 2-on-2 fold may provide sufficient rigidity to host several tunnels. High  $S^2$  parameters derived from model-free analysis and MD simulations show that motions of backbone amide vectors in trHbN are very limited on the picoseconds–nanoseconds time scale. As we already proposed, high rigidity of the backbone may enable hosting the numerous cavities that form the gas pathways connecting the DHP to the solvent.<sup>10</sup> The high rigidity of the B, E, G, and H helices on the picoseconds–nanoseconds time scale, which form the characteristic 2-on-2 helical core of the truncated hemoglobin fold, may prevent the optimization of internal side-chains van der Waals interactions that would otherwise result in tighter side-chain packing and the loss of tunnels. At the same time, the free internal volume of tunnels coupled with thermal fluctuation may allow flexibility of the side-chains making the tunnels, which is mandatory for gas migration.<sup>10,12,35–39</sup> This structural feature could also be a prerequisite in other tunnel-containing proteins. Since most of trHbN tunnel residues contain methyl groups (alanine, valine, leucine, and isoleucine), NMR characterization of these side-chain motions using  $^2\text{H}$  spin relaxation within these methyl groups may represent a great biophysical interest. For example, if NMR reveals side-chain motions for residues that appear tightly packed in MD simulations, other substrate/product diffusion routes may be formed. Afterward, new models could be tested by performing biased MD simulations techniques or by performing extended MD simulations to capture non-frequent motions.

**Dynamics in Tunnels and in the Active Site.**  $R_{\text{ex}}$  terms were observed for 13 residues located in helices B, G, and H (Figure 4B). Among these, we find the distal residue Tyr33(B10), shaping the BE tunnel, and involved in ligand binding and stabilization.<sup>15,40,41</sup> Since many catalytic processes occur on this time scale, the presence of such slow motions for this tyrosine is most likely relevant for the function of the protein.

Figure 4B also illustrates that most of the residues having a  $R_{\text{ex}}$  term are found in helix G which together with helix H define the ST tunnel and that all these residues point toward the protein core and not toward the solvent. Such colocalized slow motions could reflect the presence of a molecule slowly diffusing in the tunnels of the protein. Another potential explanation for the presence of these slow motions would be a translational movement of this helix or of the neighboring H helix in solution. Such a motion would not contribute to the NMR-derived  $S^2$ , but it would modulate the chemical shifts of amides at the interface and, depending on the time scale, would lead to the observation of  $R_{\text{ex}}$  terms in the model-free analysis. This kind of motion may increase significantly internal free volume, allowing larger substrates to penetrate the protein core. Consequently, this motion may also be necessary for bulkier  $\text{NO}_3^-$  release. Microseconds–milliseconds motions in r-trHbN could have repercussions on the dynamics and organization of the tunnel, which govern substrate/product diffusion to and out of the DHP.

We have attempted to quantify these microseconds–milliseconds motions observed from spin relaxation using CPMG relaxation dispersion experiments, without success (data not shown). This absence of dispersion in the CPMG relaxation dispersion profiles is still consistent with the  $R_{\text{ex}}$  parameters extracted from model-free analysis. Indeed, in the model-free analysis scheme we used, the contribution from microseconds–milliseconds motions on  $R_2$  is assumed to be quadratically dependent on the magnetic field strength, i.e., in the fast-exchange limit. Of course, the potential contribution from motions in the slow-exchange limit, which is independent of the magnetic field, is not totally excluded from these data. However, the flat profiles from CPMG relaxation dispersion experiments confirm that the microseconds–milliseconds motions detected from model-free analysis are most probably outside the slow-exchange limit, i.e., in the fast-exchange limit, probably with  $k_{\text{ex}} > 10\,000 \text{ s}^{-1}$  since CPMG (with  $\nu_{\text{cpmg}}$  up to 1000 Hz) could not quench the exchange.

**Pre-A “Helix” Is Not a Helix.** The main structural divergence between results from NMR and previous results from X-ray and MD concerns both the rigidity and the presence of a secondary structure for the pre-A region (residues 2–9). This region forms a somewhat unusual  $\alpha$ -helix that extends away from the globular structure in all X-ray structures of trHbN and is quite stable in MD simulations that use X-ray coordinates for an initial structure. NMR data showed no evidence for such a stable helix, or even helical propensity, in solution. Experimental data supporting disorder and the lack of secondary structure for the so-called pre-A “helix” are (1) missing or very weak resonances in the NMR spectra, attributed to potentially broadened peaks and/or fast exchange with the solvent; (2) very low  $S^2$  parameters, reflecting highly disordered N–H vectors; (3) N–H exchanging too fast to be characterized by amide exchange experiments, meaning a very low protection factor for this region (thus no or low residency H bonds); (4)

the propensity for secondary structure from chemical shifts indicates no helical conformation for this region.

The presence of such an  $\alpha$ -helical structure for the pre-A region in the trHbN X-ray structures could be favored by the high ionic strength conditions used for crystallization as well as by the crystal contacts. Indeed, careful observation of the packing of the pre-A region in the crystal lattice shows contacts with other chains which may favor an helical conformation. Although an helical conformation could potentially be transiently populated in solution, this would have to be extremely low since we saw no signs of helical propensity under the physiological conditions used for the NMR study.

Only small localized changes were observed following the removal of the pre-A region; this is in agreement with CD studies proposing that this region does not contribute to the structural integrity of the protein.<sup>16</sup> The CD data from Lama et al.<sup>16</sup> actually support a disordered pre-A model. They noted that “the content of random coil decreased when pre-A was deleted from *M. tuberculosis* HbN and increased when pre-A region was added to *M. smegmatis* HbN”. We believe that this random coil changes in their CD can be attributed to the removal/addition of a disordered pre-A region. Our pre-A results partially agree with the presence of an interaction between Arg10 and Glu70 previously detected.<sup>35</sup> Our data show that the  $C\beta$  chemical shift of Glu70 does not change upon deletion of the pre-A, hence suggesting that the environment of the Glu70 side-chain is not affected by the presence or absence of the pre-A region. As mentioned above, only two  $C\beta$  chemical shifts changes were noted upon deletion of the pre-A region, one of them being His22 (0.34 ppm shift). A potential cause for this shift may be transient polar interactions in the native protein between Glu70 (which is hydrogen bonded to His22 in the crystal structure) and one or more of the positively charged groups in the disordered pre-A (Arg6, Arg8, or Arg10), similar to the transient interaction observed by MD between Arg10 and Glu70.<sup>35</sup>

However, our data disagree with one result from the molecular dynamics simulations done by Lama et al.<sup>16</sup> In this study, it was shown that the excision of the pre-A region results in distinct changes in the protein dynamics. They observed that the Phe62(E15) gate is trapped in the closed conformation in the mutant. From our NMR data, there is no change in the amide and  $C\beta$  chemical shifts for Phe62(E15) and nearby residues in the  $\Delta$ pre-A mutant. Moreover, we have recorded  $R_2$  parameters at 600 MHz for this pre-A mutant and the  $R_2$  value observed for Phe62(E15) is the same as the mean  $R_2$  in both proteins. This implies a similar degree of slow time scale (microseconds–milliseconds) dynamics in both situations.

## CONCLUSION

This study reports the first experimental characterization of the dynamics of a truncated hemoglobin by heteronuclear NMR. The characterization of the structure and dynamics of ferric *Mycobacterium tuberculosis* trHbN bound to cyanide were done by two complementary techniques: NMR and MD simulations. This stable cyanomet form provides a good diatomic ligand system model and corresponds to the most studied form by X-ray crystallography to date. Although the nature of the hydrogen bond network with the ligand on the distal side differs slightly with that observed in the ferrous oxygen-bound structure,<sup>14</sup> X-ray crystallography and MD simulations suggest that the behavior of tunnels and pre-A conformation does not vary significantly between the oxygen–Fe(II) and cyanide–

Fe(III) forms of trHbN. Consequently, the results presented here can be extended to the more physiological oxygen–Fe(II) form.

Results obtained from both NMR and MD are in a very good agreement, validating previous results as well as our protocols. The results emphasize that trHbN is mainly rigid, especially for residues forming the 2-on-2 fold showing very limited motions of the N–H vectors in the picoseconds–nanoseconds time scale probed (average  $S^2$  for secondary structures of 0.89). Model-free analysis revealed the presence of unexpected and localized motions in the microseconds–milliseconds time scale taking place at the DHP residue Tyr33(B10) and also all along the G-helix. These motions could have important repercussions on the dynamics of the tunnels and the active site and thus on ligand diffusion and kinetics properties. Amide exchange experiments, performed at pH 7.5 and 8.5, also evidenced the very high stability of trHbN 2-on-2 fold. While X-ray structures show pre-A as an  $\alpha$ -helix,<sup>14,15</sup> our NMR data revealed this N-terminal region to be very disordered and showed no evidence for the presence of any secondary structure. The novel pre-A conformation presented here is not in contradiction with a recently proposed vital role for the pre-A region.<sup>16</sup> However, we believe it would be ill-advised to assume an helical conformation and structural order for residues 2–9 in attempting to interpret the functional role of the pre-A region. Moreover, we recommend that future MD simulations of trHbN should not be carried with an initial helical conformation for the pre-A region; an initial random conformation would likely be more accurate. Taken together, these findings are of great interest toward our understanding of trHbN function. This work could also be of interest for other gas-interaction and tunnel-containing enzymes.

Since most of trHbN tunnel residues contain methyl groups (alanine, valine, leucine, and isoleucine), a future study will characterize the  $^2\text{H}$  spin relaxation within these methyl groups in order to probe internal side-chain flexibility.

This study is thus the first step of a wide analysis of trHbN dynamics in various forms by NMR techniques.

## ■ ASSOCIATED CONTENT

### Supporting Information

Additional details, optimized CN-bound heme atomic charges,  $^{15}\text{N}$  spin relaxation data, model-free analysis results, MD-derived dynamics parameters, amide N–H bound local motions in MD simulations,  $\Delta$ pre-A  $R_2$  data,  $\Delta$ pre-A  $^1\text{H}$ – $^{15}\text{N}$  HSQC overlay, and  $\Delta$ pre-A chemical shift changes. This material is available free of charge via the Internet at <http://pubs.acs.org>.

## ■ AUTHOR INFORMATION

### Corresponding Author

\*E-mail: Stephane.Gagne@bcm.ulaval.ca. Phone: 418-656-7860. Fax: 418-656-7176.

### Present Address

<sup>§</sup>Division of Structural Biology, Biozentrum, University of Basel, Switzerland.

### Funding

This work was supported by the Natural Sciences and Engineering Research Council of Canada (NSERC), the Fonds québécois de recherche sur la nature et les technologies (FQRNT), and PROTEO, the Quebec Network for Research on Protein Function, Structure, and Engineering.

## ■ ACKNOWLEDGMENTS

The authors thank Prof. Martino Bolognesi and Olivier Fisette for stimulating discussions.

## ■ ABBREVIATIONS

NOD, nitric oxide dioxygenase; trHbN, truncated hemoglobin N; MD, molecular dynamics; NMR, nuclear magnetic resonance; *Mtb*, *Mycobacterium tuberculosis*; DHP, distal heme pocket; ST, short tunnel; LT, long tunnel; EHT, EH tunnel; BET, BE tunnel;  $\Delta$ pre-A, trHbN lacking residues 1–12; ASA, accessible surface area; r-trHbN, reconstituted trHbN; BMRB, Biological Magnetic Resonance Data Bank; rmsd, root-mean-square deviation.

## ■ REFERENCES

- Brown, G. C., and Cooper, C. E. (1994) Nanomolar concentrations of nitric-oxide reversibly inhibit synaptosomal respiration by competing with oxygen at cytochrome-oxidase. *FEBS Lett.* 356, 295–298.
- Brunori, M. (2001) Nitric oxide, cytochrome-c oxidase and myoglobin. *Trends Biochem. Sci.* 26, 21–23.
- Brunori, M., Giuffre, A., Sarti, P., Stubauer, G., and Wilson, M. T. (1999) Nitric oxide and cellular respiration. *Cell. Mol. Life Sci.* 56, 549–557.
- Cleeter, M. W. J., Cooper, J. M., Darleyusmar, V. M., Moncada, S., and Schapira, A. H. V. (1994) Reversible inhibition of cytochrome-c oxidase, the terminal enzyme of the mitochondrial respiratory-chain, by nitric-oxide - Implications for the neurodegenerative diseases. *FEBS Lett.* 345, 50–54.
- Gardner, P. R., Costantino, G., and Salzman, A. L. (1998) Constitutive and adaptive detoxification of nitric oxide in *Escherichia coli* - Role of nitric-oxide dioxygenase in the protection of aconitase. *J. Biol. Chem.* 273, 26528–26533.
- Gardner, P. R., Costantino, G., Szabo, C., and Salzman, A. L. (1997) Nitric oxide sensitivity of the aconitases. *J. Biol. Chem.* 272, 25071–25076.
- Stevanin, T. M., Ioannidis, N., Mills, C. E., Kim, S. O., Hughes, M. N., and Poole, R. K. (2000) Flavohemoglobin hmp affords inducible protection for *Escherichia coli* respiration, catalyzed by cytochromes bo' or bd, from nitric oxide. *J. Biol. Chem.* 275, 35868–35875.
- Ouellet, H., Ouellet, Y., Richard, C., Labarre, M., Wittenberg, B., Wittenberg, J., and Guertin, M. (2002) Truncated hemoglobin HbN protects *Mycobacterium bovis* from nitric oxide. *Proc. Natl. Acad. Sci. U. S. A.* 99, 5902–5907.
- Via, L. E., Lin, P. L., Ray, S. M., Carrillo, J., Allen, S. S., Eum, S. Y., Taylor, K., Klein, E., Manjunatha, U., Gonzales, J., Lee, E. G., Park, S. K., Raleigh, J. A., Cho, S. N., McMurray, D. N., Flynn, J. L., and Barry, C. E. III (2008) Tuberculous granulomas are hypoxic in guinea pigs, rabbits, and nonhuman primates. *Infect. Immun.* 76, 2333–2340.
- Daigle, R., Guertin, M., and Lague, P. (2009) Structural characterization of the tunnels of *Mycobacterium tuberculosis* truncated hemoglobin N from molecular dynamics simulations. *Proteins: Struct., Funct., Bioinf.* 75, 735–747.
- Milani, M., Pesce, A., Ouellet, Y., Dewilde, S., Friedman, J., Ascenzi, P., Guertin, M., and Bolognesi, M. (2004) Heme-ligand tunneling in group I truncated hemoglobins. *J. Biol. Chem.* 279, 21520–21525.
- Daigle, R., Rousseau, J. A., Guertin, M., and Lague, P. (2009) Theoretical Investigations of Nitric Oxide Channeling in *Mycobacterium tuberculosis* Truncated Hemoglobin N. *Biophys. J.* 97, 2967–2977.
- Golden, S. D., Olsen, K. W., and Robert, K. P. (2008) Identification of Ligand Binding Pathways in Truncated Hemoglobins Using Locally Enhanced Sampling Molecular Dynamics. *Methods Enzymol.* 437, 459–475.

- (14) Milani, M., Ouellet, Y., Ouellet, H., Guertin, M., Boffi, A., Antonini, G., Bocedi, A., Mattu, M., Bolognesi, M., and Ascenzi, P. (2004) Cyanide binding to truncated hemoglobins: a crystallographic and kinetic study. *Biochemistry* 43, 5213–5221.
- (15) Milani, M., Pesce, A., Ouellet, Y., Ascenzi, P., Guertin, M., and Bolognesi, M. (2001) Mycobacterium tuberculosis hemoglobin N displays a protein tunnel suited for O<sub>2</sub> diffusion to the heme. *EMBO J.* 20, 3902–3909.
- (16) Lama, A., Pawaria, S., Bidon-Chanal, A., Anand, A., Gelpi, J. L., Arya, S., Marti, M., Estrin, D. A., Luque, F. J., and Dikshit, K. L. (2009) Role of Pre-A motif in nitric oxide scavenging by truncated hemoglobin, HbN, of *Mycobacterium tuberculosis*. *J. Biol. Chem.* 284, 14457–14468.
- (17) Scott, N. L., and Lecomte, J. T. (2000) Cloning, expression, purification, and preliminary characterization of a putative hemoglobin from the cyanobacterium *Synechocystis* sp. PCC 6803. *Protein Sci.* 9, 587–597.
- (18) Delaglio, F., Grzesiek, S., Vuister, G. W., Zhu, G., Pfeifer, J., and Bax, A. (1995) NMRPipe: a multidimensional spectral processing system based on UNIX pipes. *J. Biomol. NMR* 6, 277–293.
- (19) Johnson, B. A., and Blevins, R. A. (1994) NMRView: A computer program for the visualization and analysis of NMR data. *J. Biomol. NMR* 4, 603–614.
- (20) Farrow, N. A., Muhandiram, R., Singer, A. U., Pascal, S. M., Kay, C. M., Gish, G., Shoelson, S. E., Pawson, T., Forman-Kay, J. D., and Kay, L. E. (1994) Backbone dynamics of a free and phosphopeptide-complexed Src homology 2 domain studied by <sup>15</sup>N NMR relaxation. *Biochemistry* 33, 5984–6003.
- (21) Kay, L. E., Keifer, P., and Saarinen, T. (1992) Pure absorption gradient enhanced heteronuclear single quantum correlation spectroscopy with improved sensitivity. *J. Am. Chem. Soc.* 114, 10663–10665.
- (22) Lipari, G., and Szabo, A. (1982) Model-free approach to the interpretation of nuclear magnetic resonance relaxation in macromolecules. 1. Theory and range of validity. *J. Am. Chem. Soc.* 104, 4546–4559.
- (23) Lipari, G., and Szabo, A. (1982) Model-Free Approach to the Interpretation of Nuclear Magnetic Resonance Relaxation in Macromolecules. 2. Analysis of Experimental Results. *J. Am. Chem. Soc.* 104, 4559–4570.
- (24) Morin, S., and Gagné, S. M. (2009) NMR dynamics of PSE-4 beta-lactamase: an interplay of ps-ns order and ms-ms motions in the active site. *Biophys. J.* 96, 4681–4691.
- (25) MacKerell, A. D., Bashford, D., Bellott, M., Dunbrack, R. L., Evanseck, J. D., Field, M. J., Fischer, S., Gao, J., Guo, H., Ha, S., Joseph-McCarthy, D., Kuchnir, L., Kuczera, K., Lau, F. T. K., Mattos, C., Michnick, S., Ngo, T., Nguyen, D. T., Prothom, B., Reiher, W. E., Roux, B., Schlenkrich, M., Smith, J. C., Stote, R., Straub, J., Watanabe, M., Wiorkiewicz-Kuczera, J., Yin, D., and Karplus, M. (1998) All-Atom Empirical Potential for Molecular Modeling and Dynamics Studies of Proteins. *J. Phys. Chem. B* 102, 3586–3616.
- (26) Brooks, B. R., Brucoleri, R. E., Olafson, B. D., States, D. J., Swaminathan, S., and Karplus, M. (1983) CHARMM: A program for macromolecular energy, minimization, and dynamics calculations. *J. Comput. Chem.* 4, 187–217.
- (27) Fisette, O., Morin, S., Savard, P.-Y., Lague, P., and Gagné, S. M. (2010) TEM-1 backbone dynamics-insights from combined molecular dynamics and nuclear magnetic resonance. *Biophys. J.* 98, 637–645.
- (28) d'Auvergne, E. J., and Gooley, P. R. (2008) Optimisation of NMR dynamic models II. A new methodology for the dual optimization of the model-free parameters and the Brownian rotational diffusion tensor. *J. Biomol. NMR* 40, 121–133.
- (29) d'Auvergne, E. J., and Gooley, P. R. (2008) Optimisation of NMR dynamic models I. Minimisation algorithms and their performance within the model-free and Brownian rotational diffusion spaces. *J. Biomol. NMR* 40, 107–119.
- (30) Volkman, B. F., Alam, S. L., Satterlee, J. D., and Markley, J. L. (1998) Solution structure and backbone dynamics of component IV Glycera dibranchiata monomeric hemoglobin-CO. *Biochemistry* 37, 10906–10919.
- (31) Bloom, M., Reeves, L. W., and Wells, E. J. (1965) Spin Echoes and Chemical Exchange. *J. Chem. Phys.* 42, xxxx.
- (32) Reddy, T., and Rainey, J. K. (2010) Interpretation of biomolecular NMR spin relaxation parameters. *Biochem. Cell Biol.* 88, 131–142.
- (33) Goodman, J. L., Pagel, M. D., and Stone, M. J. (2000) Relationships between protein structure and dynamics from a database of NMR-derived backbone order parameters. *J. Mol. Biol.* 295, 963–978.
- (34) Marsh, J. A., Singh, V. K., Jia, Z., and Forman-Kay, J. D. (2006) Sensitivity of secondary structure propensities to sequence differences between alpha- and gamma-synuclein: implications for fibrillation. *Protein Sci.* 15, 2795–2804.
- (35) Baron, R., Riley, C., Chenprakhon, P., Thotsaporn, K., Winter, R. T., Alfieri, A., Forneris, F., van Berkel, W. J., Chaiyen, P., Fraaije, M. W., Mattevi, A., and McCammon, J. A. (2009) Multiple pathways guide oxygen diffusion into flavoenzyme active sites. *Proc. Natl. Acad. Sci. U. S. A.* 106, 10603–10608.
- (36) Chen, L., Lyubimov, A., Brammer, L., Vrielink, A., and Sampson, N. (2008) The Binding and Release of Oxygen and Hydrogen Peroxide Are Directed by a Hydrophobic Tunnel in Cholesterol Oxidase. *Biochemistry* 47, 5368–5377.
- (37) Leroux, F., Dementin, S., Burlat, B., Cournac, L., Volbeda, A., Champ, S., Martin, L., Guigliarelli, B., Bertrand, P., Fontecilla-Camps, J., Rousset, M., and Léger, C. (2008) Experimental approaches to kinetics of gas diffusion in hydrogenase. *Proc. Natl. Acad. Sci. U. S. A.* 105, 11188–11193.
- (38) Saam, J., Ivanov, I., Walther, M., Holzhütter, H.-G., and Kuhn, H. (2007) Molecular dioxygen enters the active site of 12/15-lipoxygenase via dynamic oxygen access channels. *Proc. Natl. Acad. Sci. U. S. A.* 104, 13319–13324.
- (39) Tomita, A., Sato, T., Ichiyangai, K., Nozawa, S., Ichikawa, H., Chollet, M., Kawai, F., Park, S. Y., Tsuduki, T., Yamato, T., Koshihara, S. Y., and Adachi, S. (2009) Visualizing breathing motion of internal cavities in concert with ligand migration in myoglobin. *Proc. Natl. Acad. Sci. U. S. A.* 106, 2612–2616.
- (40) Ouellet, Y., Milani, M., Couture, M., Bolognesi, M., and Guertin, M. (2006) Ligand interactions in the distal heme pocket of *Mycobacterium tuberculosis* truncated hemoglobin N: roles of TyrB10 and GlnE11 residues. *Biochemistry* 45, 8770–8781.
- (41) Yeh, S. R., Couture, M., Ouellet, Y., Guertin, M., and Rousseau, D. L. (2000) A cooperative oxygen binding hemoglobin from *Mycobacterium tuberculosis*. Stabilization of heme ligands by a distal tyrosine residue. *J. Biol. Chem.* 275, 1679–1684.
- (42) Morin, S., and Gagné, S. M. (2009) Simple tests for the validation of multiple field spin relaxation data. *J. Biomol. NMR* 45, 361–372.